Surfactant sensing based on whispering-gallery-mode lasing in liquid-crystal microdroplets

M. Humar[1] and I. Muševič[1,2]*

[1] *J. Stefan Institute, Jamova 39, SI-1000, Ljubljana, Slovenia*
[2] *Faculty of Mathematics and Physics, University of Ljubljana, Jadranska 19, SI-1000, Ljubljana, Slovenia*

*igor.musevic@ijs.si

http://www.softmatter.si/

Abstract: Lasing of whispering-gallery modes in nematic liquid-crystal microdroplets, floating in water, is demonstrated. It is shown that millimolar concentrations of sodium dodecyl sulfate in water effect the orientation of liquid-crystal molecules in the microdroplet, which changes the lasing spectrum. The presence of targeted molecules in water can be monitored by simply measuring and recognizing the spectrum of light, lasing from a small liquid-crystal droplet in water.

References and links

1. P. G. de Gennes, *The Physics of Liquid Crystals* (Clarendon Press, Oxford, 1974).
2. T. Rasing, and I. Muševič, Surfaces and Interfaces of Liquid Crystals (Springer, Berlin, Heidelberg, New York, 2004).
3. J. M. Brake, M. K. Daschner, and N. L. Abbott, "Formation and characterization of phospholipid monolayers spontaneously assembled at interfaces between aqueous phases and thermotropic liquid crystals," Langmuir **21**, 2218–2228 (2005).
4. J. M. Brake, M. K. Daschner, Y. Y. Luk, and N. L. Abbott, "Biomolecular Interactions at Phospholipid-Decorated Surfaces of Liquid Crystals," Science **302**, 2094–2097 (2003).
5. Y. Y. Luk, M. L. Tingey, K. A. Dickson, R. T. Raines, and N. L. Abbott, "Imaging the Binding Ability of Proteins Immobilized on Surfaces with Different Orientations by Using Liquid Crystals," J. Am. Chem. Soc. **126**, 9024–9032 (2004).
6. C.-H. Jang, L.-L. Cheng, C. W. Olsen, and N. L. Abbott, "Anchoring of Nematic Liquid Crystals on Viruses with Different Envelope Structures," Nano Lett. **6**, 1053–1058 (2006).
7. S. Sivakumar, K. L. Wark, J. K. Gupta, N. L. Abbott, and F. Caruso, "Liquid Crystal Emulsions as the Basis of Biological Sensors for the Optical Detection of Bacteria and Viruses," Adv. Funct. Mater. **19**, 2260–2265 (2009).
8. M.I. Kinsinger, B. Sun, N.L. Abbott, and D.M. Lynn, "Reversible control of ordering transitions at aqueous/liquid crystal interfaces using functional amphiphilic polymers," Adv. Mater. **19**, 4208–4212 (2007).
9. N. A. Lockwood, J. K. Gupta, N. L. Abbott, "Self-assembly of amphiphiles, polymers and proteins at interfaces between thermotropic liquid crystals and aqueous phases," Surf. Sci. Rep. **63**, 255–293 (2008).
10. M. K. McCamley, G. P. Crawford, M. Ravnik, S. Žumer, A. W. Artstein, S. M. Opal, "Optical detection of anchoring at free and fluid surfaces using a nematic liquid crystal sensor," Appl. Phys. Lett. **91**, 141916-1–141916-4 (2007).
11. J. K. Gupta, J. S. Zimmerman, J. J. de Pablo, F. Caruso, and N. L. Abbott, "Characterization of Adsorbate-Induced Ordering Transitions of Liquid Crystals within Monodisperse Droplets," Langmuir **25**, 9016–9024 (2009).
12. E. Tjipto, K. D. Cadwell, J. F. Quinn, A. P. R. Johnston, N. L. Abbott, and F. Caruso, "Tailoring the Interfaces between Nematic Liquid Crystal Emulsions and Aqueous Phases via Layer-by-Layer Assembly," Nano Lett. **6**, 2243–2248 (2006).

13. I-H. Lin, D. S. Miller, P. J. Bertics, C. J. Murphy, J. J. de Pablo, and N. L. Abbott, "Endotoxin-Induced Structural Transformations in Liquid Crystalline Droplets," Science **332**, 1297–1300 (2011).
14. O. D. Lavrentovich, "Topological defects in dispersed words and worlds around liquid crystals, or liquid crystal drops", Liq. Cryst. **24**, 117–125 (1998).
15. K.J. Vahala, "Optical microcavities," Nature **424**, 839–846 (2003).
16. L. Novotny, and B. Hesht, *Principles of Nano-Optics* (Cambridge University Press, Cambridge, 2006).
17. A. M. Armani, R. P. Kulkarni, S. E. Fraser, R. C. Flagan, and K. J. Vahala, "Label-Free, Single-Molecule Detection with Optical Microcavities," Science **317**, 783–787 (2007).
18. M. Humar, M. Ravnik, S. Pajk, and I. Muševič, "Electrically tunable liquid crystal optical microresonators," Nat. Photonics **3**, 595–600 (2009).
19. M. L. Gorodetsky, and A. E. Fomin, "Geometrical Theory of Whispering-Gallery Modes," IEEE J. Sel. Top. Quant. **12**, 33–39 (2006).
20. M. Humar, and I. Muševič, "3D microlasers from self-assembled cholesteric liquid-crystal microdroplets," Opt. Express **18**, 26995–27003 (2010).
21. A. D. Rey, "Thermodynamics of soft anisotropic interfaces," J. Chem. Phys. **120**, 2010–2019 (2004).
22. B. D. Hamlington, B. Steinhaus, J. J. Feng, D. Link, M. J. Shelley, and A. Q. Shen, "Liquid crystal droplet production in a microfluidic device," Liq. Cryst. **34**, 861–870 (2007).
23. M. Tanyeri, R. Perron, and I. M. Kennedy, "Lasing droplets in a microfabricated channel," Opt. Lett. 32, 2529–2531 (2007).

1. Introduction

Liquid crystals (LCs) are characterized by long-range orientational order [1], where the rod-like liquid crystalline molecules are preferentially aligned along the direction, called the director. This ordering makes liquid crystals optically uniaxial materials with very large birefringence of the order of $\Delta n \sim 0.1$ and large anisotropy of material properties, such as the dielectric or diamagnetic susceptibility, elasticity and viscosity. Because of their anisotropy and soft nature, liquid crystals show a large response to the external electric and magnetic fields by collectively rotating into the direction of an applied field. In bulk, the director can point into an arbitrary direction, and free energy of a liquid crystal does not depend on the orientation. However, in the presence of confining surfaces, liquid-crystal molecules are locally forced into the direction, dictated by the local intermolecular forces at the interface. The overall LC alignment is therefore very sensitive to the strength and type of local molecular anchoring at the interface [2]. Because this surface anchoring of LC molecules strongly depends on the chemical composition of the interface, LC interfaces have successfully been used to detect, for example, phospholipids at LC-water interface [3, 4], protein binding [5], viruses [6, 7], bacteria [7] and pH measurements [8]. The long-range orientational order in LCs acts as a kind of an amplifier of the local perturbation, caused by foreign molecules, adsorbed at the interface and disturbing the interfacial ordering.

These orientational changes in the bulk liquid crystal, induced by the interfacial adsorption of foreign molecules are usually detected by observing the optical appearance of a thin layer of the liquid crystal under a polarized optical microscope [9, 10]. Typically, several micrometer thick $100\,\mu\mathrm{m} \times 100\,\mu\mathrm{m}$ layer of a liquid crystal with one surface in contact with water is used as a sensor element. The water medium provides transport of foreign species to be detected via their attachment to the LC-water interface. The reported sensitivities of such sensors are of the order of $10\,\mu\mathrm{g/ml}$ concentration in water, which corresponds to approximately one monolayer coverage of the LC interface with targeted molecules.

A flat LC sensing interface can replaced by a curved one, and the sensor is in this case a LC microdroplet dispersed in water [7, 11, 12]. Recently, it has been demonstrated that the sensitivity of such a LC microdroplet sensor can be as high as $1\,\mathrm{pg/ml}$ [13], that is at least a factor of a million better sensitivity compared to that of a flat sensing interface. It is conjectured that such an enormous amplification of the sensitivity is due to the localized binding of the targeted molecules to the point topological defects in spherical LC objects. The point

or loop-like defects must appear in curved geometry because of the topological conservation laws [14] and it takes only a few molecules to occupy the area around the point defect. While the LC microdroplets provide a new platform for ultra-sensitive biological sensors, the existing methods of the sensor readout are still impractical and are based on the bare-eye observation of the sensor under an optical microscope. We propose to use the whispering-gallery modes (WGMs) as a versatile indicator of the internal structure of the LC microdroplet. WGMs are optical eigenmodes in spherical or toroidal optical microresonators [15, 16], where the light is trapped inside a high-refractive-index microresonator because of the total internal reflection at the surfaces of the resonator. Light can be considered circulating inside the microresonator by bouncing of the interface by subsequent total internal reflections. The resonant frequency of a WGM depends on its optical path along the closed trajectory and is directly related to the profile of the refractive index along the path of the light. Any change in the profile of the refractive index, which is caused by a change of the surface boundary conditions due to the attachment of targeted molecules is therefore reflected in the spectrum of the WGMs. Since WGMs have usually very high Q-factors, already very small changes in the refractive index can be detected. The sensitivity of this method has been demonstrated by label-free, single-molecule detection by measuring the shift in the resonant frequencies when a single molecule binds to the surface of the optical microcavity [17].

In this paper, we present a new method of sensing small concentrations of targeted molecules in water by monitoring the changes in the spectra of the WGMs in LC microdroplets [18]. The spectrum of WGMs in LC microdroplets depends on the type of ordering of LC in the microdroplet and is to a larger extent determined by the orientation of liquid-crystal molecules at the water-LC interface. Foreign molecules influence this surface anchoring, which in turn changes the LC ordering inside the droplet and effects the eigenfrequencies of the WGMs. In contrast to solid WGM microresonators the molecules that bind to the LC-water interface, do not change refractive index just locally, but the perturbation is propagated into the bulk LC by long range interactions. We demonstrate that the presence of 0.3 mM concentration of sodium dodecyl sulfate (SDS) in water induces significant and clearly detectable changes in the lasing spectrum from WGMs in micrometer-sized droplets of a nematic LC. Monitoring of WGM spectra in LC microdroplets could be used as a versatile platform for easy and simple detection of small concentrations of targeted molecules in water.

2. Experimental setup

The experiments were performed using the nematic liquid crystal 4-cyano-4'-pentylbiphenyl (5CB, Nematel) doped with 0.1 wt% fluorescent dye 7-diethylamino-3,4-benzophenoxazine-2-one (Nile red, Sigma-Aldrich), which serves as a uniformly distributed light emitter. The microdroplets were produced by mechanically mixing 10 μl of dye-doped 5CB and 1 ml of 4 mM water solution of sodium dodecyl sulfate (SDS, Sigma-Aldrich). In this solution, the 5CB droplets obtain the radial distribution of the LC molecules and the SDS prevents from sticking of the droplets to the walls of the microfluidic channels, used for the measurements. The measurements were performed in a T-shaped microfluidic channel (Fig. 1) made from PDMS (Sylgard 184, Dow Corning). The channels had a rather large cross section of 1 mm × 1 mm. The dispersion of 5CB droplets in 4 mM SDS water solution was introduced in the channel. A selected 5CB droplet was trapped with an infrared laser tweezers, operating at 1064 nm (Nd:YAG, Aresis) using 60x high numerical-aperture water-immersion objective. Because the 5CB droplets could not be trapped in 3D, the droplet was pushed against the upper wall of the microchannel. As low as possible power of the trapping laser was used, typically 70 mW, not to deform or heat the droplet excessively. Further reduction of the required power was achieved by trapping the droplet not in the main channel, where the flow and the drag force were strong, but in the side
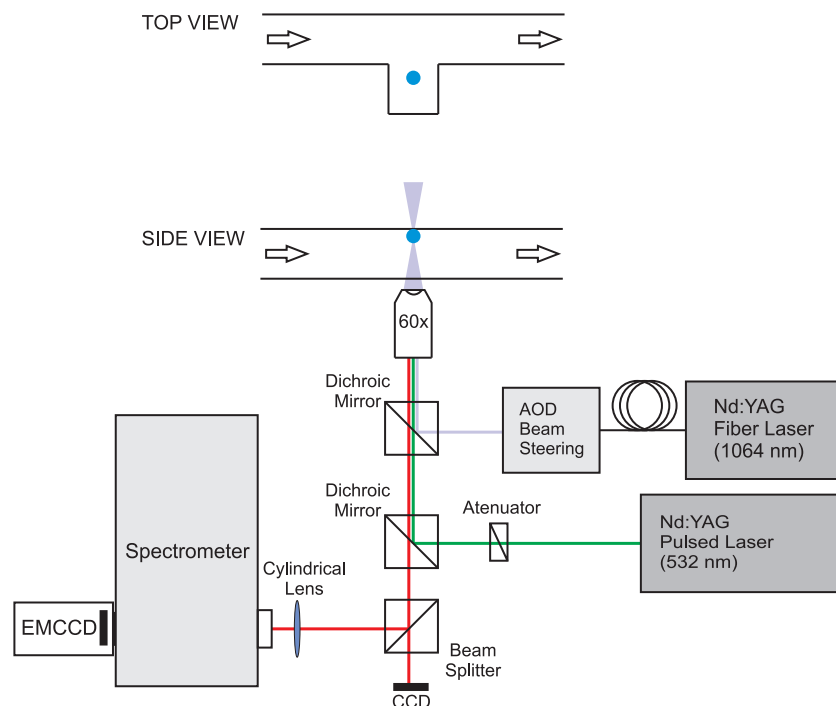
Fig. 1. The experimental setup. A selected 5CB microdroplet (blue dot, upper panel, top view) was held by the infrared laser tweezers in a blind leg of a microfluidic channel. Water with predetermined concentration of SDS was fed through the main channel at a rate of $500\,\mu$l/min. The optical setup is shown in a side view in the bottom panel. The position of the focused infrared beam is controlled by two AODs, thus allowing for the manipulation and tweezing of the 5CB droplets in water. The green pulsed beam from the doubled Nd:YAG is used to induce the fluorescence of Nile red molecules, dissolved and captured inside the 5CB droplet. The imaging spectrometer is used to measure the optical spectrum emitted by the droplet. The CCD camera is used to take the photomicrographs of the droplets.

blind leg of the the T-shaped channel, as shown in Fig. 1. In the case of non-radial director configuration in the droplet, the trapping laser rotated the droplet so, that the rotational symmetry axis was lying in the plane of the microfluidic cell, perpendicular to the direction of the laser beam. After trapping a droplet, a continuous flow of pure water was fed through the channel, so that the SDS concentration was reduced to zero. The flow flushed most droplets out of the channel except the trapped one. In pure water the droplet obtained the bipolar configuration.

After purifying the channels with water, the droplet was exposed to increasing concentrations of SDS, which was fed through the main channel at a rate of $500\,\mu$l/min. The droplet was than illuminated through the same objective by an actively Q-switched doubled Nd:YAG laser (532 nm, Alphalas, Pulselas-A-1064-500) with a pulse length of 1 ns and a repetition rate of 200 Hz. The laser light was focused to a waist diameter of $\sim 100\,\mu$m, thus illuminating the whole droplet uniformly and inducing fluorescence from the dissolved dye molecules. The emitted fluorescent light is captured inside the microdroplet in a form of WGMs, because the two refractive indices of a LC ($n_o = 1.54$ and $n_e = 1.71$) are always higher than the refractive index of water ($n = 1.33$). The spectra of the light, emitted by the droplet, was measured using an imaging spectrometer with a 0.05 nm resolution (Andor, Shamrock SR-500i) and cooled
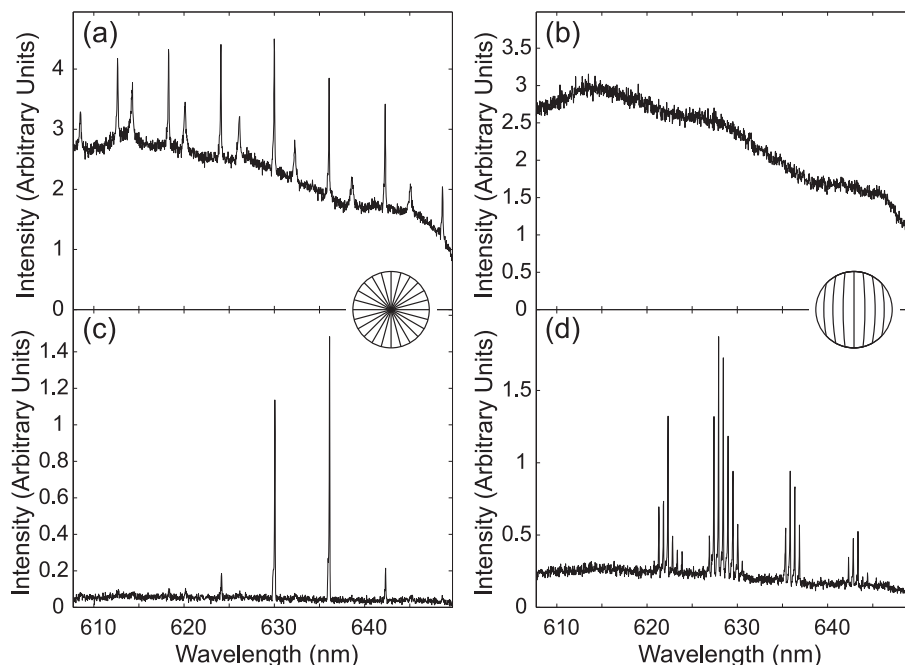
Fig. 2. Fluorescence and lasing spectra of radial and bipolar nematic microdroplets. (a) At the SDS concentration of 4 mM the 5CB droplet is in the radial configuration with a point defect in the center. The lines inside the droplet indicate molecular orientation. The fluorescence shows characteristic spectrum of WGMs. (b) In pure water with no SDS added, the 5CB droplet is in the bipolar configuration. No modes are visible in the fluorescence spectra of the microdroplet. (c) Above the lasing threshold of $0.25 \, \text{mJ/cm}^2$, lasing of the WGMs is clearly observable in the radial droplet configuration. (d) Above the lasing threshold of $0.7 \, \text{mJ/cm}^2$ several groups of lasing modes are clearly recognizable in the spectrum of 5CB microdroplet with bipolar director configuration.

EM-CCD camera (Andor, Newton DU970N). The spectra were collected every 2 s from the whole volume of the droplet.

3. Lasing characteristics

The spectrum, emitted from a $13.7 \, \mu\text{m}$ 5CB microdroplet in 4 mM SDS solution, when the droplet is in the radial nematic configuration, is shown in Fig. 2(a) and (c). At low intensity of the pumping light, sharp resonances of the WGMs in radial nematic droplets are clearly visible (Fig. 2(a)). By increasing the intensity of the pumping light, the light emission changes from the fluorescence into lasing (Fig. 2(c)). Here, some of the TM modes in Fig. 2(a) start lasing, because the light amplification is stronger than the losses of the microcavity. A similar behavior is observed for the bipolar configuration of the nematic microdroplets, which is shown in Fig. 2(b) and (d). The difference here is, that below the lasing threshold, no WGM resonances are observed (Fig. 2(b)), whereas above the lasing threshold, several groups of the WGMs are clearly observable (Fig. 2(d)). The mode splitting within each group is of the order of 0.5 nm and the width of the lasing lines is 0.05 nm, limited by the spectrometer resolution.

In spherical WGM microcavities with isotropic and uniform refractive index, the modes with different azimuthal mode numbers are degenerate. But as soon as the optical path is different in different planes of light circulation, the mode splitting occurs. The optical path difference can
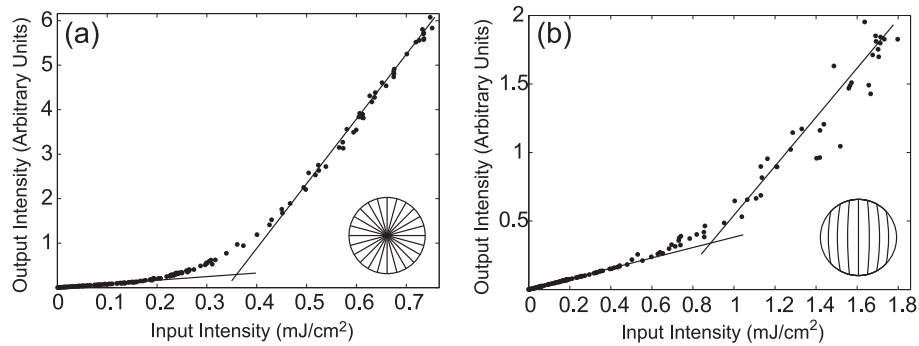
Fig. 3. The intensity of the laser line as the pump laser intensity is increased, for (a) radial 5CB nematic microdroplet and, (b) bipolar 5CB nematic microdroplet, both $13.7\,\mu$m in diameter. The lines are drawn as a guide for the eye. In both cases a clear threshold for lasing is observed.

either be a consequence of droplet deformation to a non spherical shape, or a consequence of slightly different refractive indices in different planes of circulation. From the optical micrographs of the droplets, we do not see any deformation, therefore the mode splitting can only be explained by the refractive index spatial non-uniformity. In bipolar droplets with the two defects located exactly at the interface, all orbits of light circulation very close to the interface have the same optical path. However, the difference in the optical paths emerge, as soon as the point defects (boojums) are located outside the droplet. This is possible, when the interfacial anchoring of the LC is weak. In this case, the elasticity of the distorted LC in the interior of the droplet "pushes" the two boojums out of the droplet. As an approximation to calculate the corresponding mode splitting, we used the equation for mode splitting in isotropic ellipsoids [19]. We find that the mode splitting in bipolar droplets with boojums outside the droplet corresponds to the optical path difference of 8% between the two perpendicular planes. As a comparison, the difference between the ordinary and extraordinary refractive index in 5CB is 10%.

The thresholds for lasing in the radial and bipolar configuration of a $13.7\,\mu$m 5CB microdroplet are shown in Fig. 3(a) and (b), respectively. The threshold for the radial configuration is $0.25\,\text{mJ/cm}^2$ and is approximately three times higher then for the bipolar configuration, that is $0.7\,\text{mJ/cm}^2$. The slope above the lasing threshold compared to the slope below the threshold is much steeper for radial droplets than for bipolar droplets, which agrees with the lower threshold for the radial configuration. The lasing in bipolar case is also less stable, which can be seen by scattered points above the threshold. The lasing thresholds in the WGM mode of operation are somewhat lower compared to the lasing in cholesteric droplets with Bragg-onion configuration, which is of the order of $1.2\,\text{mJ/cm}^2$, as demonstrated recently in the first 3D cholesteric liquid-crystal microlaser [20].

4. Sensing characteristics

We first observed the texture of the LC droplets under an optical microscope, and the SDS concentration was varied in steps of $0.1\,\text{mM}$. The panels in Fig. 4 show the schematic structure of the droplet (Fig. 4(a)), non-polarized microscopic images (Fig. 4(b)) and microscopic images between crossed polarizers (Fig. 4(c)) of selected $17\,\mu$m 5CB droplets at various SDS concentrations, ranging from 0 to $2\,\text{mM}$. By increasing the concentration of the surfactant, the surface anchoring continuously changes form planar to completely homeotropic [9], influencing the bulk orientation of the LC director in the droplet. At zero SDS concentration, the structure of

the droplet is bipolar, as shown in the schematic drawing in Fig. 4(a). The observed WGM splitting suggests that the LC surface anchoring is not completely planar (i.e.with molecules parallel to the curved droplet interface), but slightly tilted, so that the boojums are not on the surface, but pushed outside the droplet. The two surface boojums are indeed rarely observed in the experiment (Fig. 4(b) and (c)). By increasing the SDS concentration to 0.2 mM, the bipolar configuration transforms into a single defect loop, encircling the microdroplet at the equator (the second panel in Fig. 4(a)). After increasing the SDS concentration to 0.3 mM, the ring becomes asymmetrically positioned, shrinking first into the radial hedgehog point defect (fourth panels in Fig. 4(a), (b) and (c)). This point defect, which is located at the surface of the microdroplet then sinks into the center of the microdroplet at 2 mM concentration of SDS. The director configurations in LC droplets at different SDS concentrations match the configurations reported in previous studies [11]. The changes induced by different surfactant concentrations are completely reversible, since the surfactant molecules on the interface are in thermodynamic equilibrium with the surrounding water solution [21] and can therefore adsorb and desorb from the surface.

We have measured the concentration dependence of the light emission from 5CB microdroplets in water solution. The corresponding changes in the WGM spectra are quite significant, as shown in Fig. 4(d) and (e). For bipolar and radial droplets we have proven lasing by measuring the threshold characteristics, but for intermediate droplet configurations, the spectral lines may not always be lasing. For the bipolar droplet configuration and the inner-ring configuration up to the SDS concentration of 0.2 mM, the spectra show characteristic band-structure with a group of up to 10 lasing lines, separated by 0.5 nm. At the SDS concentration of ~ 0.2 mM, the band structure of the spectral lines starts to change. Some of the lines disappear and above 0.3 mM concentration, the lines previously forming a band, merge into a single line. The position of these merged lines shift strongly in the range of SDS concentration between 0.3 mM and 0.4 mM, and the spectrum looks quite chaotic. This chaotic spectrum changes when the droplet obtains the radial director configuration above 0.6 mM SDS concentration, and the spectra clearly shows stable lasing WGM lines, characteristic for the radial droplet structure. For the concentration range between $0.3 - 0.4$ mM, where the "chaotic" change in the spectral features occurs, a more detailed measurement was performed on a 16μm droplet by changing the concentration in 0.02 mM steps (Fig. 4(e)). Wide lines are still observed in this range, however, they change the position and width in a quite unpredictable way, not following monotonically the increasing SDS concentration.

At this stage, it is not clear how to determine the exact concentration of SDS just by measuring the spectrum in this interval of chaotic spectra. However, the lasing spectrum is sensitive to a very small variation of SDS concentration, which could potentially lead to high sensitivity. On the other hand, we can clearly distinguish the situations, where the concentration of SDS is either bellow 0.2 mM or above 0.6 mM. We expect that this concentration "window" could be pushed to significantly lower values for some targeted molecules (of the order of one millionth), such as the endotoxins. It was recently demonstrated for endotoxins [13], that already very small concentrations can induce the change from bipolar to the radial configuration. Using our WGM lasing detection technique we could in this case determine the presence of toxins in the picogram per milliliter concentrations. The LC microdroplet sensors can be also used in non-lasing regime, that is below the lasing threshold. In this case, at low surfactant concentrations, no distinct spectral lines are present, but above SDS concentration of 0.5 mM, characteristic WGM lines appear serving as an indicator for the presence of the surfactant.
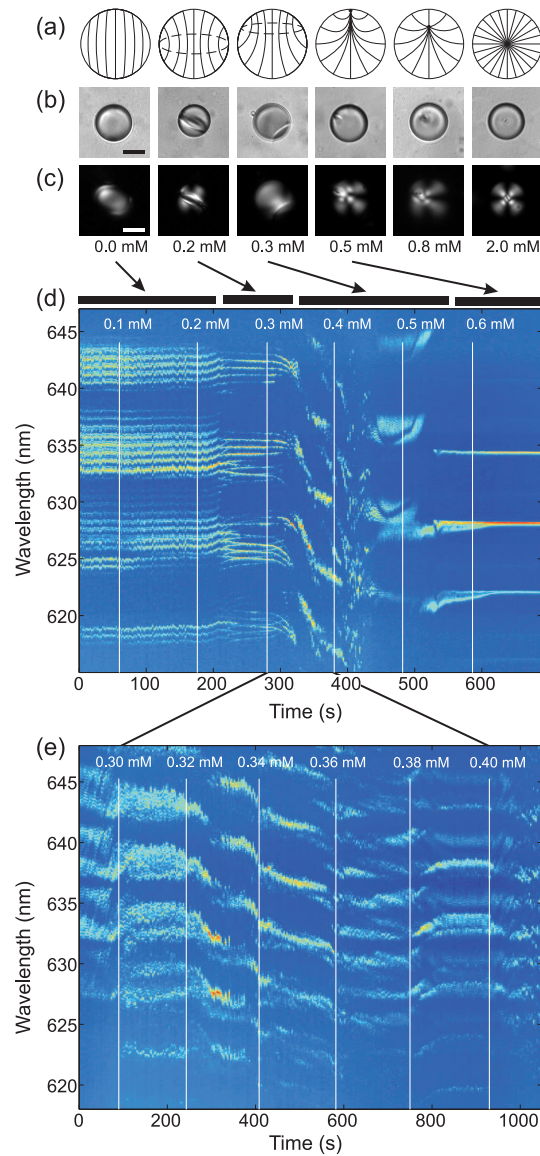
Fig. 4. Changes of the structure of a small droplet of the nematic liquid crystal at increasing concentrations of SDS. (a) The lines represent the orientation of the long axes of the LC molecules. The dots are point defects, where the orientation is not defined. In pure water, the LC molecules align parallel to the water-LC interface and the structure is bipolar. By increasing the SDS concentration, the surface anchoring of LC molecules gradually changes towards the perpendicular molecular orientation, obtained at 2.0 mM of SDS and beyond. (b) Non-polarized optical microscope images of $\sim 17\,\mu$m diameter microdroplets of 5CB in water and SDS. The "inner" ring is observable at 0.2 mM of SDS. The point defect evolves at the surface and sinks into the center at 0.8 mM concentration of SDS. Scale bar $10\,\mu$m. (c) The same images as in (b), taken between crossed polarizers. (d) The spectrum of laser light, emitted from a $13\,\mu$m 5CB droplet in water with various concentrations of SDS added. (e) Part of the lasing spectrum in the "chaotic" regime of intermediate SDS concentrations $(0.3 - 0.4\,\text{mM})$ of a $16\,\mu$m droplet.

5. Conclusion

Our results demonstrate that lasing from LC microdroplets provides for a versatile and simple method of monitoring the internal orientational structure of LC microdroplets. Because the orientation of LC inside the droplet critically depends on the anchoring of the LC at the surface of microdroplets, the lasing spectra provides direct information on the molecular adsorption/desorption processes at the surface of microdroplets. The developed sensing method could be easily integrated into existing microfluidics chips. Monodispersed LC droplets could be formed within a microchannel [22] and the excitation and detection of fluorescent light could be achieved through the integrated optical fibers [23]. Monitoring and automated recognition of the lasing spectra from LC microdroplets has therefore a clear advantage in comparison to the conventional observation of individual droplets under an optical microscope and could provide efficient and automated readout of the presence of targeted molecules in water, surrounding the LC microdroplet sensor.

Acknowledgements